ACOUSTIC PULSE SPREADING IN A RANDOM FRACTAL

KNUT SØLNA*

Abstract. Fractal medium models are used to model for instance the heterogeneous earth and the turbulent atmosphere. A wave pulse propagating through such a medium will be affected by multiscale medium fluctuations. For a class of one-dimensional fractal random media defined in terms of fractional Brownian motion we show how the wave interacts with the medium fluctuations. The modification in the pulse shape depends on the roughness of the medium and can be described in a *deterministic* way when the pulse is observed at its *random* arrival time. For very rough media the coherent wave is confined to a surface layer.

Key words. wave propagation, random medium, fractional Brownian motion, homogenization, anomalous diffusion

AMS subject classifications. 34F05, 34E10, 37H10, 60H20

1. Introduction.

Propagation of wave pulses in a *smooth* medium is well understood but propagation in a *rough* or *multiscale* medium is not so well understood. We will look at how a propagating pulse interacts with rough variations in the medium.

Given the importance and long history of wave propagation and scattering problems, a multitude of approaches have been developed to analyze them. In the homogenization or effective media regime, rapidly varying properties of the medium average out when the width of the propagating pulse is large compared to the scale of the medium fluctuations. However, over long propagation distances the accumulated effect of the scattering, associated with the medium microstructure, gradually changes the pulse *beyond* the geometrical effects of the high frequency analysis in the smooth homogenized medium. In the 1960's and early 1970's *mean* pulse propagation over long distances was analyzed. More recently a mathematical theory has been developed that gives a more precise description [1, 8, 16] of pulse propagation. It deals with pulses in a particular realization of the random medium and explains why in many cases the evolution of the *pulse shape* is to leading order *deterministic*. We refer to this phenomenon as pulse *stabilization*. So far, two salient features of this "pulse shaping" theory have been that it assumes a one dimensional medium and a separation of scales for the medium heterogeneities, that is, the medium has features on microscales which are well separated from the macroscale. However, several studies [9, 13, 14, 21] suggest that for instance the earth's crust should be modeled as containing fluctuations on a continuum of length scales. Multiscale medium models are also used for the turbulent atmosphere [20], moreover, to model the transition zone between different parts of tissues or the zone between different parts of certain devices, for instance the zone associated with a large change in the dielectric permittivity. Burridge et al. give a nice derivation of pulse shaping in periodic and stationary random media in [6]. Here, we generalize the pulse shaping theory for a two scale medium, as presented in [6], to the multiscale case.

The stabilization phenomenon has been shown to hold true also for waves propagating in three spatial dimensions in the case with layered media. This problem has been analyzed in detail in [7] and more recently also in [12] were it is discussed in the context of time-reversal of waves. Stabilization and pulse shaping in the case with slow lateral variations in the medium has been analyzed in [15] and [25].

* Department of Mathematics, University of California at Irvine, Irvine, CA 92697, (ksolna@math.uci.edu), Supported by NSF grant DMS-009399 .

The analysis of the interaction of a wave pulse with a medium varying on many length scales is an interesting but largely open question from a mathematical viewpoint; despite its importance in applications. We analyze this problem for acoustic waves propagating in a one dimensional discrete medium, modeled in terms of fractional Brownian motion. Fractional Brownian motion is a Gaussian (self-similar) stochastic processes and is often used as a model for processes containing fluctuations on a continuum of length scales, for instance for modeling of turbulent environments. The discretization assumes that the medium has a smallest scale. In turbulence theory this is the *inner* scale. Below we refer to media defined in terms of fractional Brownian motion as 'fractal' media. The Hurst exponent H characterizes the roughness of the fractional Brownian motion and the value $H = 1/2$ gives standard Brownian motion. In the simplest case with $H = 1/2$ the medium model that we consider satisfies a separation of scales assumption. For $H \neq 1/2$ the medium contains long range interactions and variations on many scales. We show that in the limit of small inner scale relative to the travel distance the transformation of the pulse shape becomes *deterministic*, thus the classic pulse shaping theory for media satisfying a separation of scales assumption generalizes in this sense. However, now the *scale* on which the spreading of the pulse happens depends on the roughness of the medium and does *not* in general correspond to the inner scale as in the classic theory. In fact, a pulse supported on the inner scale is trapped in a surface layer if the medium is rougher than the standard model. If the medium is smoother than the standard model, i.e. $H > 1/2$, the shape of such a pulse is *not* affected by the random medium fluctuations.

Most previous work on wave interaction with a fractal object deals with scattering caused by fractal interfaces. However, some authors have explored wave-interaction with deterministic fractal media using numerical simulations [4, 17, 26]. Reflections from a random fractal and how they depend on the fractal exponent is explored by numerical experiments in [4]. In [17] Konotop et al. examine the wave reflections from a fractal devil's staircase and introduce a heuristic scheme for computing effective parameters of such a medium. Sun et al. [26] explore numerically wave propagation in a similar medium and observe strong resonance effects. Here, we analyze acoustic pulse transmission through a random fractal and illustrate our theoretical results with numerical simulations.

In Section 2 we state the governing equations for the acoustic pulse and in Section 3 the models for the fractal media that we consider. We summarize how the pulse shaping theory generalizes to these media in Section 4. In Section 5 we derive the general averaging result that can be used for fractal media. Finally, in Section 6, we apply this averaging result to the fractal media that we consider and also illustrate our theoretical results with numerical simulations.

2. Governing equations. We follow the notation set forth in [3] and [6]. The governing equations for the continuum are the Euler equations giving conservation of momentum and mass

$$\begin{aligned} \rho\, u_t + p_z &= 0 \\ K^{-1} p_t + u_z &= 0 \end{aligned} \tag{1}$$

with t being time and z measuring depth into the medium. The dependent variables are the pressure p and the (z-component) of the particle velocity u. The medium parameters are the density ρ and the bulk-modulus K, which is the reciprocal of the compressibility. We next make a change of variables from depth z to the first arrival

time from the surface to this depth:

$$x = x(z) \;=\; \int_0^z \frac{1}{c(s)}\, ds, \tag{2}$$

with the local speed of sound being $c = \sqrt{K/\rho}$. The first arrival time gives the travel time for the first arriving disturbances. An important aspect of the propagating pulse is the travel time of its *coherent* part and this differs in general from the first arrival time. In travel time coordinates (1) transforms into

$$\begin{aligned} \zeta u_t + p_x &= 0 \\ p_t + \zeta u_x &= 0. \end{aligned} \tag{3}$$

The characteristic impedance ζ is

$$\zeta = \zeta(x) \;=\; \sqrt{\rho(z(x))\; K(z(x))} \;=\; \rho(z(x))\; c(z(x)) \tag{4}$$

where $z(x)$ is the inverse of the map defined in (2).

We model ζ as being piecewise constant, thus, within each medium section the wave propagation can be described as a pure translation of 'up'- and 'down'-propagating wave components. We decompose the wavefield in terms of up- and down-propagating wave components as

$$\begin{aligned} u &= \frac{1}{\sqrt{\zeta}}\; (D - U) \\ p &= \sqrt{\zeta}\; (D + U). \end{aligned} \tag{5}$$

The positive x direction defines the downward direction and D is the wave propagating in this direction. Our objective is to describe a down-propagating pressure pulse somewhere deep into the medium and examine how the multiscale random fluctuations in ζ affects this pulse. In Section 3 we give the particular models that we consider for the medium fluctuations and in Section 4 discuss their impact on the transmitted pulse.

3. Modeling of the medium. The discrete medium is defined by a *uniform* discretization in the travel time coordinate x as

$$\zeta = \begin{cases} 1 & \text{for } \; x < h \\ \zeta_k^h & \text{for } \; (k-1)\; h \le x < k\; h \end{cases} \tag{6}$$

with $k \in \{1, 2, \cdots\}$. Therefore, the time it takes a pulse to traverse a medium section is constant and equal to h. Such a medium is sometimes referred to as a Goupillaud medium, it has been discussed in for instance [6], [22] and [24]. Here, we consider finely layered media and h is the small parameter in our modeling. In the next section we describe our choices for the impedance sequence ζ_k^h, the sequence that defines the medium.

3.1. A standard onescale medium model. We first consider a medium model where the fluctuations form a stationary process with the impedances in the different medium sections being independent and identically distributed. Such a medium model is used in [5, 6, 16]. Let the discrete impedance sequence be given by

$$\zeta_k^h = 1 + Z_k^h, \tag{7}$$

with Z_k^h a sequence of independent mean zero Gaussian random variables with variance $\mathcal{O}(h)$. The medium fluctuations are therefore relatively weak. Note that in practice we truncate the fluctuations in the above model such that the impedance is positive and bounded. If β denotes standard Brownian motion, then a version of (7) can be constructed as

$$\zeta_k^h = 1 + \beta(kh) - \beta((k-1)h). \tag{8}$$

This formulation serves to motivate the medium model we introduce next; a model that incorporates fluctuations on many scales.

3.2. Multiscale medium from Fractional Brownian noise. We aim to formulate a simple medium model that incorporates long range interactions or correlations, that is, a model that is not limited to one intrinsic scale as the one in (8). A standard stochastic model process that incorporates long range interactions and variations on a continuum of lengh scales is fractional Brownian motion (fBm), $\{\beta_H(x); x \geq 0\}$. This process was introduced by Mandelbrot and Van-Ness in [18]. We define the medium model in terms of this process.

First, consider the following generalization of (8)

$$\zeta_k^h = 1 + \beta_H(kh) - \beta_H((k-1)h) \tag{9}$$

with β_H being fBm with Hurst exponent H. Thus, the fluctuations in the impedance is a fBm *noise* sequence. Note that $\beta_{1/2}$ is standard Brownian motion and then the models (8) and (9) coincide. In general, fBm is a Gaussian process with mean zero, stationary increments and with covariance and structure functions

$$E[\beta_H(x)\beta_H(y)] = \frac{\sigma^2}{2}(|x|^{2H} + |y|^{2H} - |x-y|^{2H}) \tag{10}$$

$$E[(\beta_H(x) - \beta_H(x-\Delta x))^2] = \sigma^2 |\Delta x|^{2H} \tag{11}$$

where $0 < H < 1$, σ a scaling parameter and $\beta_H(0) = 0$. The Hurst exponent H determines the correlation of the increments. The covariance of a future increment with the past increment is

$$E[(\beta_H(x) - \beta_H(x-\Delta x))(\beta_H(x+\Delta x) - \beta_H(x))] = \sigma^2(2^{2H-1} - 1)|\Delta x|^{2H}$$

and is independent of the location index x. When $H > 1/2$ this quantity is positive so if the past increment is positive, then on average the future increment will be positive. Feder [10] calls this persistence. When $H < 1/2$ we have an antipersistent process with a positive increment in the past making a positive increment in the future less likely. The paths of fBm in the persistent case will be associated with larger excursions, but will be 'smoother' than the paths in the antipersistent case. The quadratic variation of the process in the persistent case is almost surely zero whereas it is almost surely infinite in the antipersistent case [23]. Below we show how this entails that wave propagation through a medium defined in terms of antipersistent fBm is qualitatively very different from wave propagation in the persistent case.

In the model (8) the impedance is piecewise constant and ζ_k^h are uncorrelated with ζ_{k+m}^h unless $m = 0$. We refer to this model as a one scale model whose scale of variation corresponds to the discretization scale.

In this section we consider a model for the impedance that has long range correlations, the covariane is now:

$$C_\zeta(m;h,H,\sigma) := Cov[\zeta_k^h, \zeta_{k+m}^h] \ \sim \ \frac{\sigma^2 h^{2H} H(2H-1)}{m^{2(1-H)}} \quad \text{as } m \ \to \ \infty,$$

and the medium therefore exhibits correlations also over long scales. Note that if we observe the medium on a coarser scale then we see the same decay of correlations, for $a > 0$:

$$C_\zeta(am; h, H, \sigma) \sim a^{-2(1-H)} C_\zeta(m; h, H, \sigma) \quad \text{as } m \to \infty.$$

Since the medium has similar and nontrivial correlation structure over many scales we refer to it as a multiscale model.

In fact, fBm itself is self-similar since $\beta_H(x)$ and $a^H \beta_H(x/a)$ have the same finite dimensional distributions for all $a > 0$. This property illustrates how this process incorporates variations on all scales.

3.3. A fractal medium model. The model (9) is defined in terms of fractional Gaussian noise and the medium fluctuations are therefore stationary. Next, we define a medium model where the fluctuations are defined by the fractional Brownian motion process itself. In this case the fluctuations are nonstationary, moreover, they are strong $\mathcal{O}(1)$ and not weak as in the above two models. We consider the medium model

$$\zeta_k^h = \exp(\beta_H(kh)). \tag{12}$$

The value $H = 1/3$ is of particular interest since the fBm process then corresponds to Kolmogorov turbulence, a standard medium model in the context of wave propagation in the turbulent atmosphere. We will see below that the same theorem, Theorem 5.1, that characterizes the transformation of the pulse shape for the models in the previous two subsections with weak or small medium fluctuations applies in this case with relatively strong medium fluctuations. Below, in (16), we introduce the interface reflection coefficients associated with the sequence ζ_k^h. The theorem characterizes how the decay of the correlations in these interface reflection coefficients determines how the medium affects the shape of the propagating wave pulse. The important parameters that determines this decay is the Hurst exponent H, and the pulse shaping thus depends sensitively on the value of this. We give the decay of correlations for the interface reflection coefficients in (41). Note that even though the fluctuations of the impedance in (12) are large, the magnitude of the fluctuations of the interface reflection coefficients are actually small.

Observe finally that the analysis we present below holds for more general media models than those discussed above.

4. Summary of results. In this section we characterize the wave pulse that has propagated through the multiscale medium. We assume the model (9) and in addition that the density ρ in (4) is constant. This allows us to characterize the travel time to a given depth. The general case is considered in (5.1). We give a more detailed account for the results and how they are derived in Sections 5 and 6.

The pulse impinging on the halfspace $z > 0$ has shape p_0, a compactly supported function. In the *random* medium the transmitted pulse at depth L can be characterized in terms of (i) $\chi_h(L)$ a *random* travel time correction. (ii) $\mathcal{G}$ a *deterministic* pulse shaping function. The support of $\mathcal{G}$ is $\mathcal{O}(\sqrt{L})$. Let $\tau(L)$ be the travel time to depth $z = L$ in the deterministic (homogenized) medium, then we have the following result for the transmitted pulse

LEMMA 4.1. *Let* $1/4 < H \leq 1/2$ *and* $p(0,t) = p_0(t/h^{H+1/2})$ *be the impinging*

pulse at the surface. Then for every $\varepsilon > 0$ *and* $M > 0$,

$$\mathbb{P}(\sup_{|s|<M} |p(L,\tau(L)+\chi_h(L)+h^{H+1/2}s) - \int p_0(s-u)\mathcal{G}(u;L)\ du| > \varepsilon) \to 0 \quad as \quad h \to 0. \tag{13}$$

The random variable χ_h is a Gaussian random variable with magnitude $\mathcal{O}(h)$. Thus, when we observe the transmitted pulse in a randomly corrected time frame we see a deterministic pulse in the small h limit. This is what we refer to as *stabilization*. If $H = 1/2$, then β_H is standard Brownian motion that has independent increments, corresponding to independent medium fluctuations. In this case the spreading of the pulse happens on the diffusion scale h which is a measure of the correlation length of the medium fluctuations, Spreading on this scale corresponds to the one discussed by O'Doherty and Anstey in [19]. If $H < 1/2$, the increments of β_H are *negatively* correlated and the medium fluctuations are rougher than in the standard Brownian case. In this case the pulse shaping is stronger and happens on the anomalous diffusion scale $h^{H+1/2}$.

Consider next the case that $H > 1/2$, now the increments of β_H are *positively* correlated and the medium fluctuations are smoother than in the standard Brownian case. The next result shows that in this case there is no change in pulse shape on the discretization scale in the small h limit.

LEMMA 4.2. *Let* $H > 1/2$ *and* $p(0,t) = p_0(t/h)$ *be the impinging pulse at the surface. Then for every* $\varepsilon > 0$ *and* $M > 0$,

$$\mathbb{P}(\sup_{|s|<M} |p(L,\tau(L)+\chi_h(L)+hs) - p_0(s)| > \varepsilon) \to 0 \quad as \quad h \to 0. \tag{14}$$

The travel time correction χ_h is characterized as in Lemma 4.1.

Assume that the source pulse is supported on the inner scale: $p_0 = p_0(t/h)$. In the Brownian case with $H = 1/2$ it follows from Lemma 4.1 that on the standard diffusion scale h we observe stabilization to a *fixed* pulse shape at the *fixed* depth L. If $H < 1/2$ with a stronger pulse shaping this result generalizes in that we see stabilization on the scale h to a fixed pulse, but for a travel distance that *decreases* with h. Analogously, for $H > 1/2$, with a weaker pulse shaping, we observe stabilization on the scale h for a travel distance that *increases* with decreasing h. This follows from

LEMMA 4.3. *Let* $1/4 < H < 3/4$ *and* $p(0,t) = p_0(t/h)$ *be the impinging pulse at the surface. Then for every* $\varepsilon > 0$ *and* $M > 0$,

$$\mathbb{P}(\sup_{|s|<M} |p(Lh^{1-2H},\tau(Lh^{1-2H})+\chi_h(L)+hs) - \int p_0(s-u)\mathcal{G}(u;L)\ du| > \varepsilon) \to 0 \ as\ h \to 0. \tag{15}$$

Thus, the coherent pulse front will be confined to an $\mathcal{O}(Lh^{1-2H})$ neighborhood of the surface. The random variable χ_h is a Gaussian random variable, now with magnitude $\mathcal{O}(h^{1+H(1-2H)})$.

5. Derivation of pulse shaping.

5.1. Dynamic equations for the pulse front. In order to derive the above results we need to characterize the evolution of the pulse front and how this relates to

the fluctuations in the impedance ζ. Wave propagation in the discrete medium is determined by the interface reflection coefficients, r_k^h, and the transmission coefficients, τ_k^h. These are defined by

$$r_k^h = \frac{\zeta_{k+1}^h - \zeta_k^h}{\zeta_{k+1}^h + \zeta_k^h} \tag{16}$$

$$\tau_k^h = \sqrt{1 - |r_k^h|^2}. \tag{17}$$

Let $D^{\pm}$ and $U^{\pm}$ be the wave components in (5) evaluated immediately to the right and left of interface k at location $x_k = kh$. The interface corresponds to a jump in the characteristic impedance ζ and continuity of p and u gives the appropriate interface conditions that determine the associated jumps in D and U. These jumps correspond to some of the down-propagating energy being converted to the up-propagating mode and visa versa. The interface conditions give [6]

$$\begin{bmatrix} D^+ \\ U^- \end{bmatrix} = \begin{bmatrix} \tau_k^h & -r_k^h \\ r_k^h & \tau_k^h \end{bmatrix} \begin{bmatrix} D^- \\ U^+ \end{bmatrix}. \tag{18}$$

We are interested in the impulse response of the medium. That is, how a down-propagating impulse at the surface is being transformed as it propagates. The impulse response is an analogue of the Green's function for the medium. The transmitted pulse when we probe the medium with a general *down*-propagating wave is easily found by convolution of the source wave with this impulse response. At the initial time we assume that the medium is at rest and that we probe it with a down-propagating impulse:

$$\begin{aligned} D_{t=0} &= \delta(x^+) \\ U_{t=0} &= 0. \end{aligned} \tag{19}$$

Wave reflections at the interfaces in the discrete medium lead to a set of down- and up-propagating impulses. At the time instances $t = ih$, with i integer, these impulses are located at the interfaces. The down-propagating pulses are separated by integer multiples of h in the time coordinate, t, and also in the travel time coordinated, x; as are the up-propagating impulses. We find it convenient to represent these 'impulse-trains' by the magnitude of the impulses indexed as D_j^i and U_j^i, with i being the time index and corresponding to times $t = ih$. The index j gives the distance from the front in the x dimension, measured in units of h. Thus, D_0^i is the magnitude of the first impulse in the down-propagating pulse-train at time $t = ih$. The initial condition (19) gives

$$\begin{aligned} D_j^0 &= \delta_0(j) \\ U_j^0 &= 0. \end{aligned} \tag{20}$$

In **Figure 1** we illustrate the propagation of the impulses by a sequence of 'snapshots' taken at times $t = 0, h$ and $2h$. The figure makes it clear that at time instances $t = ih$ only every second interface are associated with non-zero impulses and that the support of the pulse-trains increases with increasing time, giving pulse spreading. An important aspect of the parameterization is that a finite section of the wave front evolves autonomously and can be described independently of the tail part of the wave. We make use of this fact for the analysis of the problem and also for numerical

simulation of the evolution of the wave front. Consider D_2^2 in the example given in Figure 1. That is, the magnitude of the second down-propagating impulse, at time $2h$. It trails the leading impulse by two sections and is determined by a double scattering event associated with the initial impulse D_0^0. Part of the initial impulse is first reflected to an up-propagating mode and then aligned with D_2^2 through a second scattering event. The change in D_{2j} from one time step to the next can in general be expressed *exactly* in terms of double scattering events associated with down-propagating impulses 'ahead' of it when these are evaluated at previous times. We next show how by unraveling the evolution seen in Figure 1.

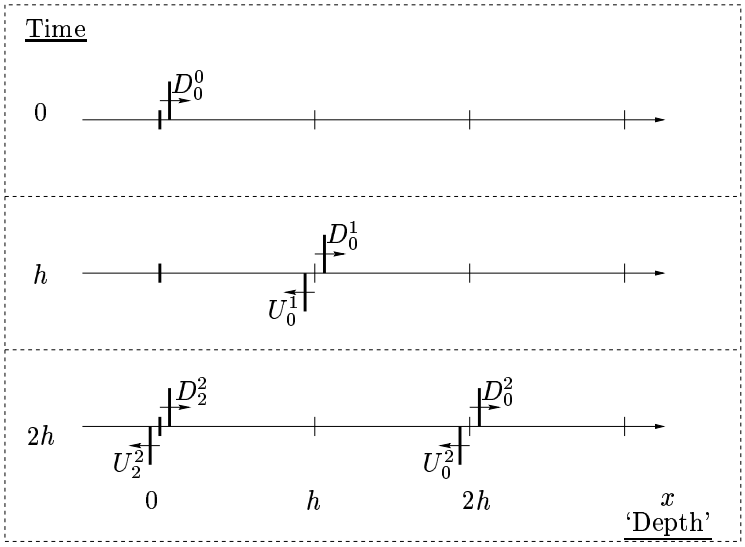

FIG. 1. *The figure illustrates the generation of multiple reflections in the discrete medium.*

From (18) we find

$$\begin{bmatrix} D_j^{i+1} \\ U_j^{i+1} \end{bmatrix} = \begin{bmatrix} \tau_k^h & -r_k^h \\ r_k^h & \tau_k^h \end{bmatrix} \begin{bmatrix} D_j^i \\ U_{j-2}^i \end{bmatrix} \tag{21}$$

with $k = i + 1 - j$. Define

$$d_j^i = \prod_{k=0}^{i-j} \tau_k^h \; D_j^i \tag{22}$$

$$u_j^i = \prod_{k=0}^{i-j-1} \tau_k^h \; U_j^i$$

with $\tau_k^h = 1$ for $k < 0$. This gives using (18) that

$$d_j^{i+1} = d_j^i - r_k^h u_j^{i+1}$$
$$u_j^{i+1} = u_{j-2}^i + r_k^h d_j^i,$$

with $k = i + 1 - j$. Then, upon elimination of u_j^i it follows in view of (20) that

$$\mathbf{d}^{i+1} = \mathbf{d}^i - \mathbf{A}_i^h \mathbf{d}^i \tag{23}$$

with the vector $\mathbf{d}^i$ corresponding to the front part of the wave:

$$\mathbf{d}^i = [d_0^i, d_2^{i+1}, d_4^{i+2}, \cdots]'.$$

The matrix $\mathbf{A}_i^h = \{a_{k,l}^i\}$ is *lower-triangular* with

$$a_{k,l}^i = r_{i-k+2}^h \; r_{i-l+2}^h \tag{24}$$

for $k \geq l$. In the next section we use (23) to obtain a characterization of the transmitted pulse. Note that (23) articulates how the change in a down-propagating impulse at a given time can be expressed exactly in terms of double scattering events associated with impulses 'ahead' of it when these are evaluated at previous times. Thus, the statistics of products of reflection coefficients, corresponding to these double scattering events, will determine the evolution of the pulse shape.

5.2. Stabilization from averaging. We state the conditions and the result that describes the fascinating stabilization property of the down-propagating pulse when this is observed in a travel-time frame. With stabilization we mean that the transmitted pulse becomes essentially deterministic in the small h limit due to averaging in (23). Averaging in (23) means that we can replace $\mathbf{A}_i^h$ by its mean value which is a lower triangular Toeplitz matrix with the entries on the $i'th$ subdiagonal being $E[r_m^h r_{m+i}^h]$, assuming here that the interface reflection coefficients form a stationary sequence. The following theorem generalizes and makes this precise.

Let $[\cdot]$ denote rounding to integer value, and define

$$\begin{aligned} \frac{d\mathcal{D}}{ds}(s,h) &= -\bar{\mathbf{A}}(s,h)\; \mathcal{D}(s,h) \\ \mathcal{D}(0,h) &= \mathbf{e}_1 \end{aligned} \tag{25}$$

with $\bar{\mathbf{A}}(s,h)$ being a lower triangular Toeplitz matrix whose first column is

$$[a(0, s/g(h), h)/2, a(1, s/g(h), h), \cdots, a(K, s/g(h), h)]'$$

for some function a and $\mathbf{e}_1$ a vector with one in the first entry and zero else, moreover

$$\begin{aligned} \mathbf{D}(x,h) &= [D_0^{[x/h]}, D_2^{[x/h]}, \cdots, D_{2K}^{[x/h]}]' \\ \mathbf{U}(x,h) &= [U_0^{[x/h]}, U_2^{[x/h]}, \cdots, U_{2K}^{[x/h]}]' \; , \end{aligned} \tag{26}$$

with D_j^i and U_j^i as defined above, then,

THEOREM 5.1. *If for all $\epsilon > 0$ and $\Delta \in \{0, 1, 2 \cdots\}$*

$$\lim_{h\to 0} \mathbb{P}[\sup_{0<s<L} | \sum_{m=1}^{[s/(g(h)h)]} r_m^h r_{m+\Delta}^h - \int_0^s a(\Delta, v/g(h), h)\; dv| > \epsilon] = 0, \tag{27}$$

where $0 < g(h)h = o(1)$ and $|a| < c$ for some constant c, then for all $\epsilon > 0$

$$\lim_{h\to 0} \mathbb{P}[\sup_{0<s<L} ||\mathbf{D}(s/g(h), h) - \mathcal{D}(s,h)|| > \epsilon] = 0 \tag{28}$$

$$\lim_{h\to 0} \mathbb{P}[\sup_{0<s<L} ||\mathbf{U}(s/g(h), h)|| > \epsilon] = 0. \tag{29}$$

The proof of this result is given in Appendix C. The formulation (25) follows from replacing $\mathbf{A}_i^h$ in (23) and the factor $\prod_{k=1}^m \tau_k^h$ in (22) by their corresponding averaged values. We apply the above result to fractal media in Section 6.

The following lemma shows that the condition (27) entails that the interface reflection coefficients are small. Note, however, that this does not mean that the medium fluctuations themselves are relatively small.

LEMMA 5.2. *If for all* $\epsilon > 0$ *and* $\Delta \in \{0, 1, 2 \cdots\}$

$$\lim_{h\to 0} \mathbb{P}[\sup_{0<s<L} |\sum_{m=1}^{[s/(g(h)h)]} r_m^h r_{m+\Delta}^h - \int_0^s a(\Delta, v/g(h), h)\, dv| > \epsilon] = 0 \tag{30}$$

where $0 < g(h)h = o(1)$ *and* $|a| < c$ *for some constant* c, *then for all* $\epsilon > 0$

$$\lim_{h\to 0} \mathbb{P}[\sup_{1\le i\le [L/(g(h)h)]} |r_i^h| > \epsilon] = 0. \tag{31}$$

We prove this lemma in Appendix A.

For a given random medium model the following lemma gives a convenient way to check that the condition (27) is satisfied. Define

$$S^h(s,\Delta) = \sum_{m=1}^{[s/(g(h)h)]} r_m^h r_{m+\Delta}^h - \int_0^s a(\Delta, v/g(h), h)\, dv, \tag{32}$$

then

LEMMA 5.3. *With* a *and* g *defined as in (27), if there is an* $\alpha > 0$ *and a* $C > 0$ *such that for* $h < h_0$

$$\sup_{0<s<t<L} E[|S^h(t,\Delta) - S^h(s,\Delta)|^\alpha] \le g(h)h|t-s|C \tag{33}$$

then the condition (27) is satisfied.

The proof of this lemma can be found in Appendix B.

Theorem 5.1 shows how the shape of the transmitted pulse is affected by the medium fluctuations. In the next section we give an interpretation of this modification and show that for an important class of random media models the spreading of the pulse in the random medium can be described as a convolution with a deterministic Gaussian pulse shape.

5.3. Pulse shape from the Central Limit Theorem. Assume first that the interface reflection coefficient are stationary and that:

$$E[r_i^h\ r_{i+\Delta}^h] = ha(\Delta).$$

It then follows from Theorem 5.1 that in probability $\lim_{h\to 0} \mathbf{D}(L,h) = \mathcal{D}(L)$ with

$$\mathcal{D}(L) = \exp(-L\bar{\mathbf{A}})\ \mathbf{e}_1 \ = \ \exp(-La(0)/2)\exp(La(0)\mathcal{Q}/2)\ \mathbf{e}_1$$

where $\bar{\mathbf{A}}$ and $\mathcal{Q}$ are lower triangular Toeplitz matrix whose first columns are

$$\mathbf{a} = [a(0)/2,\ a(1),\ a(2), \cdots]'$$
$$\mathbf{q} = -[0,\ 2a(1)/a(0),\ 2a(2)/a(0), \cdots]'$$

respectively. Note that multiplication with $\mathcal{Q}$ corresponds to a discrete convolution with its first column. Therefore

$$\mathcal{D}(L) = \sum_{n=0}^{\infty} p_n \mathbf{q}^{n*} \qquad as \quad h \downarrow 0 \tag{34}$$

where $\mathbf{q}^{n*}$ denote n-fold convolution, $\mathbf{q}^0 = e_1$, and where

$$p_n = \exp(-La(0)/2)(La(0)/2)^n/n!$$

is a discrete Poisson distribution. For typical media models, for instance when ζ_k^h form a Markov process, the first column of $\mathcal{Q}$ define a discrete probability distribution. Then $\mathcal{D}$ is the distribution of a *random sum.* A Central Limit Theorem argument then gives that $\mathcal{D}$ is approximately a Gaussian pulse shape with standard deviation $\mathcal{O}(\sqrt{L})$ for L large. We show this in Appendix F where we consider media with slowly varying media statistics.

6. Application to a fractal environment. In this section we consider the multiscale medium models introduced in Sections 3.2 and 3.3. We show how Theorem 5.1 applies to these media and give the medium statistics that define the deterministic transformation in the shape of the propagating pulse. The results presented in Section 4 follow via a transformation from the travel time coordinate to physical depth.

6.1. Fractional Brownian noise medium. We consider the medium model (9). A calculation involving the algebra of the moments of Gaussian random variables gives Lemma 6.1 below.

LEMMA 6.1. *Let ζ_k^h be defined by (9) and $1/4 < H < 3/4$ then $\exists \;\; h_0 > 0$ such that*

$$\lim_{h\to 0} E[\sum_{m=1}^{[s/g(h)h]} r_m^h r_{m+\Delta}^h] = sa(\Delta) \tag{35}$$

$$Var[\sum_{m=1}^{[s/g(h)h]} r_m^h r_{m+\Delta}^h] \le g(h)hs\sigma^4 C(H) \quad for \;\; h \le h_0 \tag{36}$$

with $g(h) = h^{2H-1}$ and for $\Delta \ge 1$

$$\begin{aligned} a(\Delta) &= -\Delta^{2H-4} \; (\sigma^2/8) \; \delta_{1/\Delta}^4 [x^{2H}]_{x=1} \\ &\sim -\Delta^{2H-4} \; \sigma^2 \; H(H-1/2)(H-1)(2H-3) \;\; as \;\; \Delta \to \infty. \end{aligned} \tag{37}$$

In (37) we used the forth order discrete central difference operator δ_Δ^4 defined by

$$\delta_\epsilon[f(x)] = \frac{f(x+\epsilon/2) - f(x-\epsilon/2)}{\epsilon}.$$

Thus, the coefficients $a(\cdot)$ can be expressed in terms of a forth order difference operator of the power law of the underlying fBm. This is related to the fact that these coefficients are means of products of interface reflection coefficients that themselves are obtained essentially by discrete differentiation of the impedance sequence. Lemmas 5.3 and 6.1 entail that the condition (27) in Theorem 5.1 is satisfied for the model (9) with $g(h) = h^{2H-1}$. Thus, in probability, the transmitted impulse response when evaluated at depth $\tilde{L} = Lh^{1-2H}$ satisfies

$$\begin{aligned} \lim_{h\to 0} \mathbf{D}(\tilde{L}/h, h) &= \exp(-L\bar{\mathbf{A}}) \; \mathbf{e}_1 \\ \lim_{h\to 0} ||\mathbf{U}(\tilde{L}/h, h)|| &= 0 \end{aligned} \tag{38}$$

where $\bar{\mathbf{A}}$ is a lower triangular Toeplitz matrix whose first column is

$$[a(0)/2,\ a(1),\ a(2), \cdots]$$

and $\mathbf{U}$ and $\mathbf{D}$ are defined in (26). Thus, when we probe the medium with a unit downgoing impulse at the surface we observe the pulse shape defined by (38) at depth $\tilde{L}$. By a transformation of the independent variable to physical depth this entails that Lemmas 4.2 and 4.3 in Section 4 are valid when the fractal medium is defined by (9). That Lemma 4.1 holds follows from Lemmas 5.3 and 6.1 and from Theorem 5.1 upon a transformation of the travel time argument.

We next illustrate these results regarding the model (9) with numerical simulations. In the numerical simulations we use the initial condition (19) and propagate the pulse essentially according to (23). In practice we reformulate (23) to obtain an orthogonal propagation operator. In the figures we plot the down-propagating pulse $\mathbf{D}$ at the considered depth. Note that the origin in the plotted coordinate system corresponds to the front of the pulse, that is D_0^N with N the total number of sections in the discrete medium. Thus, in the absence of random medium fluctuations we will only see a unit impulse at the origin. The random medium variations cause a spreading of the impulse.

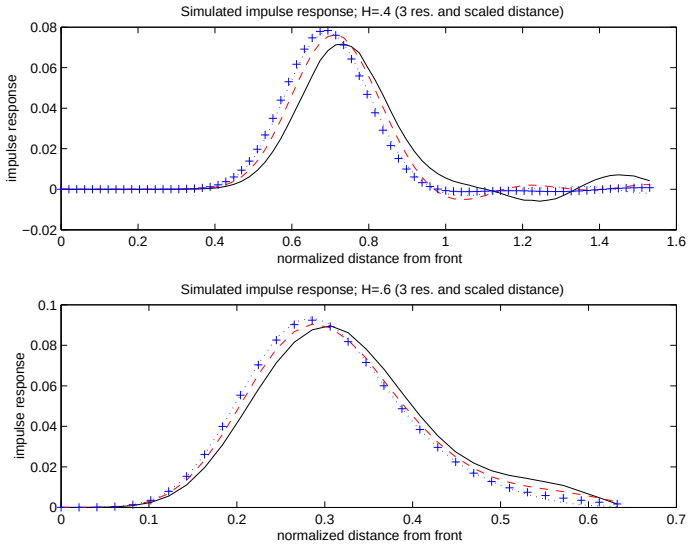

FIG. 2. *The figure shows the impulse response of the fractal medium plotted at a depth that* scales *with the inner scale* h *as* h^{1-2H}. *The horizontal axis is scaled by* h. *In this frame we see stabilization to a fixed pulse in the small* h *limit. This limit is approximately a Gaussian pulse shape. In the top plot* $H = .4$ *and in the bottom* $H = .6$. *The medium model is the one defined in (9). The solid, dashed and dotted lines correspond to* $h_0 = 2^{-12}$, $h_1 = 2^{-14}$ *and* $h_2 = 2^{-16}$ *respectively. The crosses give the theoretical pulse shapes.*

First, we illustrate Lemma 4.3 using the medium model (9). In **Figure 2** we use $\sigma = 5$ and the solid, dashed and dotted lines correspond to $h_0 = 2^{-12}$, $h_1 = 2^{-14}$ and $h_2 = 2^{-16}$ respectively. The pulses are plotted at the scaled depth

$$\bar{x}(h_i) = \left(\frac{h_i}{h_0}\right)^{1-2H}.$$

The crosses give the stabilized pulse shaped defined by (34). In the top plot we use $H = 0.4$ whereas we use $H = 0.6$ in the bottom plot. As expected we see stabilization to the theoretical pulse in both cases. Note that the horizontal axis is scaled by h. The pulse shaping is stronger in the antipersistent case with a rougher medium (top plot). The limiting pulse shape is close to the Gaussian pulse shape. This can be explained by the representation (34) of the impulse response. Recall that if the vector $\mathbf{q}$, the first column of $\mathcal{Q}$, is non-negative then (34) can be interpreted as the distribution of a random sum and the impulse response will be close to the Gaussian pulse shape. The vector $\mathbf{q}$ is non-negative for $H \geq 1/2$ giving in the small h limit a Gaussian pulse as in the bottom plot. For $H < 1/2$ the sequence $\mathbf{q}$ is partly negative. In the top plot we used a value for the Hurst exponent that is slightly smaller than the Brownian case, $H = 0.4$, and the pulse shape is close to the Gaussian shape. Note that since the pulses are plotted at depth $\propto h^{1-2H}$ we have to go shallower and shallower in the case $H < 1/2$ to see the stabilized pulse. This corresponds to an antipersistent fBm and to rough medium variations. In the persistent case with $H > 1/2$ and a smoother medium we have to go deeper and deeper into the medium to see the stabilized pulse. Only in the pure Brownian case with $H = 1/2$ do we observe the pulse stabilization at a *fixed* depth.

Next, we illustrate Lemmas 4.1 and 4.2 using the medium model (9). In **Figure 3** we plot the same impulse responses as in Figure 2, only evaluated at the fixed depth $L = 1$. As expected, in the small h limit the impulse response in the case $H = .4 < 1/2$ (top plot) approaches a stabilized Gaussian pulse shape. Note that the impulse responses are plotted relative to the scale $h^{2H} = h^{.8}$. This is the scale at which the pulse shape stabilizes in the small h limit. The crosses give the limiting pulse shape and conform closely with the numerical simulations. The bottom plot shows the transmitted impulses when $H = .6 > 1/2$. Then the impulse response becomes close to a unit impulse for small h. The figure shows that the numerical impulse responses approach, albeit slowly, the unit impulse as h is reduced.

In **Figure 4** we show how the impulse response depends rather sensitively on the value of the Hurst exponent H that gives the roughness of the medium. We use $h = 2^{-16}$, $L = 1$, $\sigma = 1$ and the model defined in (9). The solid curve corresponds to the Kolmogorov scaling law with $H = 1/3$. The dotted and dashed lines correspond respectively to a 20% increase/decrease in the Hurst exponent, giving less respectively more spreading of the pulse.

6.2. The fractal case. Next, we let ζ_k^h be defined by the medium model in (12). Observe therefore that the medium fluctuations are strong and $\mathcal{O}(1)$ in contrast to the models considered above where they were small. However, we will find that the interaction with the medium fluctuations can be characterized in a similar way as above. The following lemma can be shown by a generalization of the analysis that leads to Lemma 6.1.

LEMMA 6.2. *Let ζ_k^h be defined by (12) and $1/4 < H < 3/4$ then*

$$\lim_{h\to 0} E[\sum_{m=1}^{[s/g(h)h]} r_m^h r_{m+\Delta}^h] = sa(\Delta) \tag{39}$$

$$Var[\sum_{m=1}^{[s/g(h)h]} r_m^h r_{m+\Delta}^h] \leq g(h)hs\sigma^4 C(H) \quad \textit{for} \quad h \leq h_0 \tag{40}$$

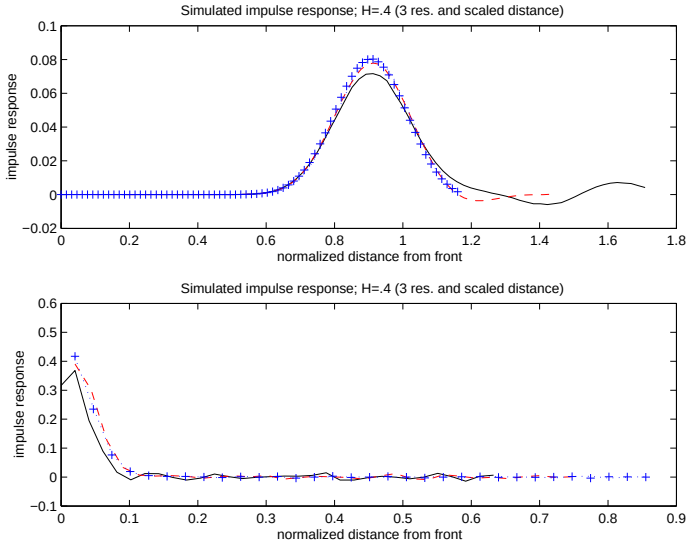

FIG. 3. *The figure shows the impulse response of the fractal medium plotted at a* fixed *depth. The horizontal axis is scaled by* h^{2H}. *The top plot illustrates stabilization to a Gaussian pulse on the relative scale* $h^{2H} = h^{.8}$, *the bottom stabilization to the unit impulse. As above, in the top plot* $H = .4$ *and in the bottom* $H = .6$. *The medium model is the one defined in (9). The solid, dashed and dotted lines correspond to* $h_0 = 2^{-12}$, $h_1 = 2^{-14}$ *and* $h_2 = 2^{-16}$ *respectively. The crosses give the theoretical pulse shapes corresponding to the smallest* h *value.*

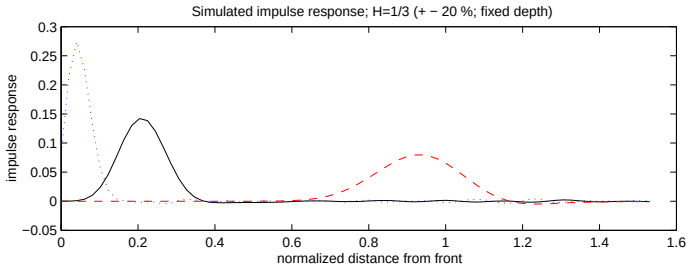

FIG. 4. *The figure shows the impulse response of the fractal medium plotted at a* fixed *depth. It illustrates how the pulse shaping depends on the value of the Hurst exponent* H *that gives the roughness of the medium. The solid line corresponds to* $H = 1/3$ *and the dotted and dashed lines to a 20% increase respectively decrease. The medium model is the one defined in (9).*

with $g(h) = h^{2H-1}$ *and for* $\Delta \geq 1$

$$a(\Delta) = \sigma^2 \Delta^{2H-2}\ \delta^2_{1/\Delta}[x^{2H}]_{x=1}/8 \tag{41}$$
$$\sim \Delta^{2H-2}\ \sigma^2 H(H-1/2)/2 \quad as \quad \Delta \to \infty.$$

Note that now the impedance is defined in terms of the fBm process itself rather than fBm noise and that the $a(\cdot)$ coefficients thus is defied in terms of a second rather than forth order difference operator. We show below that this has a strong effect on the impulse response. Lemma 6.2 entails that the condition (27) in Theorem 5.1 again is satisfied with $g(h) = h^{2H-1}$. Thus, in probability, the transmitted impulse response when evaluated at depth $\tilde{L} = Lh^{1-2H}$ satisfies (38) where $\bar{\mathbf{A}}$ is a lower triangular Toeplitz matrix whose first column is $\mathbf{a}' = [a(0)/2,\ a(1),\ a(2), \cdots]$ with $a(\cdot)$ now

defined by (41).

Figure 5 corresponds to Figure 2 only that we used the model (12) with $\sigma = 1$. The impulse response is again plotted relative to the scale h and at depth

$$\bar{x}(h_i) = \left(\frac{h_i}{h_0}\right)^{1-2H}.$$

Again we observe stabilization in this frame. The solid, dashed and dotted lines correspond to $h_0 = 2^{-12}$, $h_1 = 2^{-14}$ and $h_2 = 2^{-16}$ respectively. In the top plot $H = .4$ and in the bottom plot $H = .6$. The transformation of the pulse shape is weaker than above due to the smoother medium fluctuations. The crosses give the theoretical pulse shapes and these conform closely with the numerical simulations for small h. In this case with a fractal medium the correlations decay slower than for the medium discussed in the previous section, as can be seen from (37) and (41). The second moment associated with the discrete distribution $\mathbf{q}$, defined as the first column of $\mathcal{Q}$ in (34), is now unbounded and the Central Limit Theorem not valid for this distribution. Thus, the pulse shape does not approach the Gaussian shape as it did above. Due to the long range interactions in the medium fluctuations the scattered wave energy is now spread far out and the coherent part of the pulse reduced in amplitude, but not much in its shape.

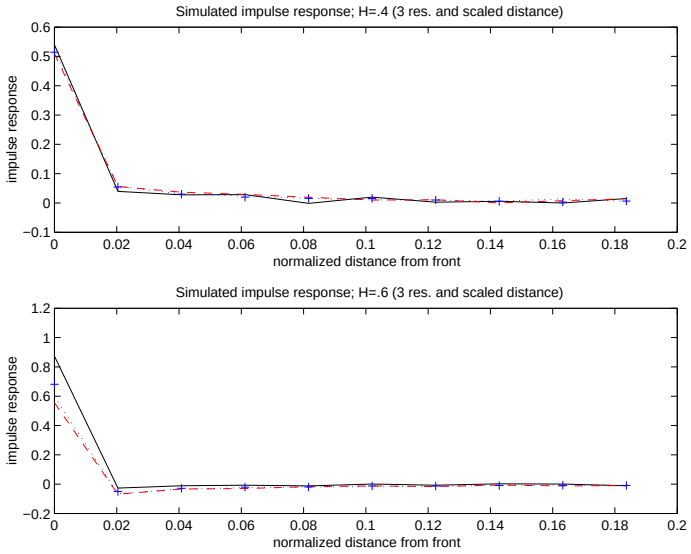

FIG. 5. *The Figure corresponds to Figure 2 only that medium model (12) rather than (9) is used. The figure shows the impulse response of the fractal medium plotted at a depth that* scales *with the inner scale h as* h^{1-2H} *and the horizontal axis is scaled by h. In this frame we see stabilization to a fixed pulse in the small h limit. In the top plot* $H = .4$ *and and in the bottom* $H = .6$. *The solid, dashed and dotted lines correspond to* $h_0 = 2^{-12}$, $h_1 = 2^{-14}$ *and* $h_2 = 2^{-16}$ *respectively.*

REFERENCES

[1] Asch M., W. Kohler, G. C. Papanicolaou, M. Postel and B. White, *Frequency content of randomly scattered signals*, SIAM Review, V 33, 519-625, (1991).

[2] Billingsley P., *Probability and measure* , John Wiley & Sons, (1986).
[3] Bube K. P. and R. Burridge, *The one-dimensional inverse problem of reflection seismology*, SIAM Review, V 25, 497-559, (1983).
[4] Bulgakov S. A., V. V. Konotop and L. Vazquez, *Wave interaction with a random fat fractal: dimension of the reflection coefficient*, Waves in Random Media, V. 5, 9-18, (1995).
[5] Burridge R., P. Lewicki and G. C. Papanicolaou, *Pulse stabilization in a strongly heterogeneous layered medium*, Wave Motion, V 20, 177-195, (1994).
[6] Burridge R., G. C. Papanicolaou and B. S. White, *One dimensional wave propagation in a highly discontinuous medium*, Wave Motion, V 10, 19-44, (1988).
[7] Chillan J. and J. P. Fouque, *Pressure fields generated by acoustical pulses propagating in randomly layered media*. SIAM Journal on Applied Math., V 58, 1532-1546, (1998).
[8] Clouet J. F. and J. P. Fouque, *Spreading of a pulse traveling in random media.*, Annals of Applied Probability, V 4, 1083-1097, (1994).
[9] Crossley D. J. and O. G. Jensen, *Fractal velocity models in refraction seismology*, Pageoph., V 131, 61-76, (1989).
[10] Feder J. *Fractals*, New York: Plenum Press, (1988).
[11] Feller W., *An introduction to probability theory and its applications* , John Wiley & Sons, (1971).
[12] Fouque J.P. and K. Sølna, *Time-reversal aperture enhancement*, submitted, (2002).
[13] Herrmann F., *A scaling medium representation, a discussion on well-logs, fractals and waves*, PhD thesis, Delft University of Technology, (1997).
[14] Hewett T. A., *Modeling reservoir heterogeneities with fractals*, Proc. 4th International Geostatistics Congress, Terra Abstracts, 4, Suppl. 3, 9, (1992)
[15] Kohler W., G. Papanicolaou and B. White *Reflection and transmission of acoustic waves by a locally-layered slab.*, In: Diffuse Waves in Complex Media, edited by Jean-Pierre Fouque, Math and Physical Sciences Series vol 531, Kluwer, The Netherlands, 347-382, (1999).
[16] Lewicki P., R. Burridge and M. V. de Hoop, *Beyond Effective Medium Theory: Pulse Stabilization for Multimode Wave Propagation in High Contrast Layered Media.*, SIAM Journal on Applied Math., V 56, 256-276, (1996).
[17] Konotop V. V., Z. Fei and L. Vazquez, *Wave interaction with a fractal layer*, Physical Review E, V 48, 4044-4048, (1993).
[18] Mandelbrot B. B. and J. Van Ness, *Fractional Brownian motion, fractional noises and applications*, SIAM Rev., V 10, 422-437, (1968).
[19] O'Doherty R. F. and N. A. Anstey, *Reflections on amplitudes*, Gephysical Prospecting 19, 430-458, (1971).
[20] Papanicolaou G. and K. Sølna *Wavelet based estimation of Kolmogorov turbulence*, In Long-range Dependence: Theory and Applications, P. Doukhan, G. Oppenmeim and M. S. Taqqu, editors, Birkhauser, 2002.
[21] Pilkington M. and J. P. Todoeschuck, *Stochastic inversion for scaling geology*, Geophys. J. Int., V 102, 205-217, (1990).
[22] Richards P. G. and W. Menke, *The apparent attenuation of a scattering medium*, Bull. Seism. Soc. Amer. 73, 1005-1021, (1983).
[23] Rogers L. C. G., *Arbitrage with fractional Brownian motion*, Math. Finance, V 7, 95-105, (1997).
[24] Sølna K., *Focusing of time-reversed reflections*, Waves in Random Media, 12, 365-385, (2002).
[25] Sølna K. and G. Papanicolaou, *Ray theory for a locally layered medium*, Waves in Random Media, V 10, 155-202, (2000).
[26] Sun X. and D. L. Jaggard, *Wave interaction with a generalized Cantor bar fractal multilayers*, J. Applied Phys., V 70, (1991).

Appendix A. Magnitude of medium fluctuations.

We prove Lemma 5.2 stated in Section 5. This lemma shows that the condition (27) entails that in the small h limit the interface reflection coefficients are small.

First, observe that the condition (27) allows us, for any given $\epsilon > 0$, to choose h_0 so small that for $h < h_0$

$$\mathbb{P}[\sup_{0<s<L} |\sum_{m=1}^{[s/(g(h)h)]} |r_m^h(\omega)|^2 - \int_0^s a(0, v/g(h), h)\, dv| > \epsilon^2/4] < \epsilon/2. \tag{42}$$

Now let $\{h^j\}$ be a sequence such that $\lim_{j\to\infty} h^j = 0$. Denote the associated array of interface reflection coefficients $r_i^{h^j}(\omega),\ 1 < i < N^j$ with

$$N^j = [L/(g(h^j)h^j)].$$

Assume that Lemma 5.2 is *false*. Then there is a subsequence $\{h^j\}$ of the above kind, a fixed $\epsilon > 0$ and a sequence of collections of disjoint sets $\{\mathcal{F}_i^j\}_{i=1}^{N_j}$ so that

$$\mathbb{P}\left[\bigcup_i \mathcal{F}_i^j\right] = \sum_{i=1}^{N_j} \mathbb{P}[\mathcal{F}_i^j] \ > \ \epsilon$$

with

$$|r_i^{h^j}(\omega)| > \epsilon \ \text{ for } \ \omega \in \mathcal{F}_i^j. \tag{43}$$

We next show that this leads to a contradiction. Define

$$f(s;j) := S^{h_j}(s,0) = \sum_{m=1}^{[s/(g(h^j)h^j)]} |r_m^{h^j}(\omega)|^2 - \int_0^s a(0, v/g(h^j), h^j)\ dv.$$

Note that $f(s;j)$ has a jump discontinuity at

$$s_{(i;j)} := ig(h^j)h^j,$$

that is

$$f(s_{(i;j)}^+; j) - f(s_{(i;j)}^-; j) = |r_i^{h^j}(\omega)|^2.$$

For $1 \le i \le N^j$ we therefore find

$$\sup_{0<s<L} \Big| \sum_{m=1}^{[s/g(h^j)h^j]} |r_m^{h^j}(\omega)|^2 - \int_0^s a(0, v/g(h^j), h^j)\ dv \Big| \ = \ \sup_{0<s<L} |f(s;j)|$$
$$\ge \ \frac{|f(s_{(i;j)}^+; j) - f(s_{(i;j)}^-; j)|}{2} \ = \ \frac{|r_i^{h^j}(\omega)|^2}{2},$$

and for $\omega \in \mathcal{F}_i^j$ it follows

$$\sup_{0<s<L} \Big| \sum_{m=1}^{[s/g(h^j)h^j]} |r_m^{h^j}(\omega)|^2 - \int_0^s a(0, v/g(h^j), h^j)\ dv \Big| \ > \ \frac{\epsilon^2}{2}. \tag{44}$$

We can thus conclude that:

$$\mathbb{P}[\sup_{0<s<L} \Big| \sum_{m=1}^{[s/g(h^j)h^j]} |r_m^{h^j}|^2 - \int_0^s a(0, v/g(h^j), h^j)\ dv \Big| > \epsilon^2/4] \ge \sum_{i=1}^{N_j} \mathbb{P}[\mathcal{F}_i^j] \ > \ \epsilon$$

contradicting (42).

Appendix B. A stabilization criterion.

In this appendix we prove Lemma 5.3 stated in Section 5. To prove Lemma 5.3 we need to show that (33) implies that for $\epsilon > 0$ and $\delta > 0$ there is an h_0 such that for $h < h_0$

$$\mathbb{P}[\sup_{0<s<L} |S^h(s,\Delta)| \geq \epsilon] \leq \delta \tag{45}$$

with S^h defined by (32):

$$S^h(s,\Delta) = \sum_{m=1}^{[s/(g(h)h)]} r_m^h r_{m+\Delta}^h - \int_0^s a(\Delta, v/g(h), h)\ dv. \tag{46}$$

Observe first that we can choose $\bar{h}$ so small that for $h < \bar{h}$:

$$g(h)h \sup_{(\Delta,v,h)} a(\Delta, v, h) < \epsilon/2 \tag{47}$$

since $|a|$ is bounded and $g(h)h = o(1)$. From (46) it follows that for $h < \bar{h}$ and i integer:

$$\mathbb{P}[\sup_{0<s<L} |S^h(s,\Delta)| \geq \epsilon] \leq \mathbb{P}[\sup_{0\leq i\leq [L/(g(h)h)]} |S^h(ig(h)h,\Delta)| \geq \epsilon/2].$$

Therefore, to show (45) we need to show that for h small enough:

$$\mathbb{P}[\sup_{0\leq i\leq [L/(g(h)h)]} |S^h(ig(h)h,\Delta)| \geq \epsilon/2] \leq \delta. \tag{48}$$

In the rest of this section we suppress the dependence on Δ.

The result (48) follows from two bounds that we will derive below from (33). For i and j integers we have the following two bounds. First

$$\frac{2L}{\bar{\Delta}} \sup_{0\leq i\leq [L/\bar{\Delta}]} \mathbb{P}[\sup_{0\leq j\leq [\bar{\Delta}/(g(h)h)]} |S^h(i\bar{\Delta} + jg(h)h) - S^h(i\bar{\Delta})| \geq \epsilon/4] \leq \delta/2 \tag{49}$$

for

$$\bar{\Delta} = \min\left[\frac{(\delta/2)(\epsilon/4)^\alpha}{2LC}, L\right] \tag{50}$$

with the quantities involved being defined as in Lemma 5.3. Second

$$\mathbb{P}[\sup_{0\leq i\leq [L/\bar{\Delta}]} |S^h(i\bar{\Delta})| \geq \epsilon/4] \leq \delta/2 \tag{51}$$

for

$$h \leq \mathcal{H}[\frac{\bar{\Delta}(\delta/2)(\epsilon/4)^\alpha}{L(L+\bar{\Delta})C}] \tag{52}$$

with

$$\mathcal{H}(v) = \begin{cases} \infty & \text{if } \sup_h(g(h)h) < v, \\ \inf_h \ | \ [g(h)h > v] & \text{else} \end{cases}.$$

From (49) and (51) we can conclude that (48) is indeed satisfied for ϵ small if

$$h \leq \mathcal{H}[\frac{(\delta/2)^2(\epsilon/4)^{2\alpha}}{4L^3C^2}],$$

and $\bar{\Delta}$ is chosen as in (50) because then

$$\begin{aligned}
&\mathbb{P}[\sup_{0\leq i\leq[L/(g(h)h)]} |S^h(ig(h)h)| \geq \epsilon/2] \\
&\leq \sum_{i=0}^{[L/\bar{\Delta}]} \mathbb{P}[\sup_{0\leq j\leq[\bar{\Delta}/(g(h)h)]} |S^h(i\bar{\Delta}+jg(h)h) - S^h(i\bar{\Delta})| \geq \epsilon/4] \\
&\quad +\mathbb{P}[\sup_{0\leq i\leq[L/\bar{\Delta}]} |S^h(i\bar{\Delta})| \geq \epsilon/4] \\
&\leq \frac{2L}{\bar{\Delta}} \sup_{0\leq i\leq[L/\bar{\Delta}]} \mathbb{P}[\sup_{0\leq j\leq[\bar{\Delta}/(g(h)h)]} |S^h(i\bar{\Delta}+jg(h)h) - S^h(i\bar{\Delta})| \geq \epsilon/4] + \delta/2 \ \leq \ \delta.
\end{aligned}$$

We now show (49). Define first the event

$$A(j;i) = [\ |S^h(i\bar{\Delta}+jg(h)h) - S^h(i\bar{\Delta})| \geq \epsilon/4]$$

Observe that then

$$\begin{aligned}
&\mathbb{P}[\sup_{0\leq j\leq[\bar{\Delta}/(g(h)h)]} |S^h(i\bar{\Delta}+jg(h)h) - S^h(i\bar{\Delta})| \geq \epsilon/4] \\
&= \mathbb{P}[\bigcup_{j=1}^{[\bar{\Delta}/(g(h)h)]} A(j;i)] \ \leq \ \sum_{j=1}^{[\bar{\Delta}/(g(h)h)]} \mathbb{P}[A(j;i)].
\end{aligned}$$

Using Chebyshev's inequality and (33) we find

$$\mathbb{P}[A(j;i)] \leq \frac{E[|S^h(i\bar{\Delta}+jg(h)h) - S^h(i\bar{\Delta})|^\alpha]}{(\epsilon/4)^\alpha} \ \leq \ \frac{Cj(g(h)h)^2}{(\epsilon/4)^\alpha}.$$

Therefore, we can conclude

$$\begin{aligned}
&\mathbb{P}[\sup_{0\leq j\leq[\bar{\Delta}/(g(h)h)]} |S^h(i\bar{\Delta}+jg(h)h) - S^h(i\bar{\Delta})| \geq \epsilon/4] \\
&\leq \frac{\bar{\Delta}}{g(h)h} \sup_{1\leq j\leq[\bar{\Delta}/(g(h)h)]} \mathbb{P}[A(j;i)] \ \leq \ \frac{\bar{\Delta}}{g(h)h} \frac{C\bar{\Delta}g(h)h}{(\epsilon/4)^\alpha} \ = \ \frac{C\bar{\Delta}^2}{(\epsilon/4)^\alpha}.
\end{aligned}$$

Thus, (49) is satisfied for $\bar{\Delta}$ given as in (50).

Consider next showing (51). Note that

$$\mathbb{P}[\sup_{0\leq i\leq[L/\bar{\Delta}]} |S^h(i\bar{\Delta})| \geq \epsilon/4] \leq \left[\frac{L}{\bar{\Delta}}+1\right] \sup_{0\leq i\leq[L/\bar{\Delta}]} \frac{E[|S^h(i\bar{\Delta})|^\alpha]}{(\epsilon/4)^\alpha} \ \leq \ \left[\frac{L}{\bar{\Delta}}+1\right] \frac{CLg(h)h}{(\epsilon/4)^\alpha}.$$

Thus, (51) is satisfied if

$$\frac{(L+\bar{\Delta})LCg(h)h}{\bar{\Delta}(\epsilon/4)^\alpha} \leq \delta/2$$

or

$$g(h)h \leq [\frac{\bar{\Delta}(\delta/2)(\epsilon/4)^{\alpha}}{L(L+\bar{\Delta})C}]$$

which gives (52).

Appendix C. Stabilization.

We prove Theorem 5.1 given in Section 5. Let $\mathbf{X}_i^h$ satisfy

$$\begin{aligned} \mathbf{X}_{i+1}^h &= (\mathbf{I} - \mathbf{A}_i^h)\ \mathbf{X}_i^h \\ \mathbf{X}_0^h &= \mathbf{I} \end{aligned} \tag{53}$$

with $\mathbf{A}_i^h$ defined in (23) and $\mathbf{X} \in \mathbb{R}^{[K]\times[K]}$. We show: for all $\epsilon > 0$

$$\lim_{h\to 0} \mathbb{P}[\sup_{0<s<L} ||\mathbf{X}_{[s/(g(h)h)]}^h - \mathbf{X}(s)|| > \epsilon] = 0 \tag{54}$$

where

$$\begin{aligned} \frac{d\mathbf{X}(s)}{ds} &= -\mathcal{A}(s,h)\ \mathbf{X}(s) \\ \mathbf{X}(0) &= \mathbf{I} \end{aligned} \tag{55}$$

and $\mathcal{A}$ is a lower triangular Toeplitz matrix whose first column is

$$[a(0, s/g(h), h), a(1, s/g(h), h), \cdots, a(K, s/g(h), h)]'$$

and with the function a being defined as in (25).

In order to show (54) we introduce a continuous version of $\mathbf{X}_i^h$. Let $\mathbf{X}^h(s)$ satisfy

$$\begin{aligned} \frac{d\mathbf{X}^h(s)}{ds} &= -\mathcal{A}^h(s)\ \mathbf{X}^h(s) \\ \mathbf{X}^h(0) &= \mathbf{I} \end{aligned}$$

with

$$\mathcal{A}^h(s) = -\frac{1}{g(h)h}\ln(\mathbf{I} - \mathbf{A}_i^h) \quad \text{for} \quad (i-1)g(h)h \ \leq\ s\ \leq\ ig(h)h,$$

then $\mathbf{X}^h(ig(h)h) = \mathbf{X}_i^h$, (note that in view of Lemma 5.2 we can truncate the elements of $\mathbf{A}$).

Next, define the residual

$$\tilde{\mathbf{X}}^h(s) = \mathbf{X}^h(s) - \mathbf{X}(s).$$

Making use of an integrating factor and that

$$\begin{aligned} \frac{d\mathbf{X}^{-1}(s)}{ds} &= \mathbf{X}^{-1}(s)\mathcal{A}(s,h) \\ \mathbf{X}^{-1}(0) &= \mathbf{I} \end{aligned} \tag{56}$$

we find

$$\begin{aligned} \tilde{\mathbf{X}}^h(s) = &-\int_0^s \tilde{\mathcal{A}}^h(v)\ dv\ \mathbf{X}^h(s) - \int_0^s \mathbf{X}(s)\ \mathbf{X}^{-1}(v) \int_0^v \tilde{\mathcal{A}}^h(v')\ dv'\ \mathcal{A}^h(v)\ \mathbf{X}^h(v)\ dv \\ &+ \int_0^s \mathbf{X}(s)\ \mathbf{X}^{-1}(v)\ \mathcal{A}(v,h)\ \int_0^v \tilde{\mathcal{A}}^h(v')\ dv'\ \mathbf{X}^h(v)\ dv \end{aligned} \tag{57}$$

with

$$\tilde{\mathcal{A}}^h(v) = \mathcal{A}^h(v) - \mathcal{A}(v,h).$$

From (31) it follows that $\forall\ \epsilon > 0$

$$\lim_{h\to 0} \mathbb{P}[\sup_{1\le i\le [L/(g(h)h)]} ||\mathbf{A}_i^h|| > \epsilon] = 0. \tag{58}$$

Moreover, from (27) it follows that $\forall \epsilon > 0$

$$\lim_{h\to 0} \mathbb{P}[\sum_{i=1}^{[s/(g(h)h)]} |\mathbf{A}_i^h(k,l)| - 2\int_0^s a(0, s/g(h), h)ds > \epsilon] = 0 \tag{59}$$

with $\mathbf{A}_i^h(k,l)$ being the elements of the matrix $\mathbf{A}_i^h$. Given a $c_1 > 0$ we find using (58) that $\exists\ c_2 > 0$ such that $\forall\ \delta > 0\ \ \exists\ h_0 > 0$ so that

$$\mathbb{P}[\int_0^s ||\mathcal{A}^h(v)||dv > c_1] \le \mathbb{P}[\sum_{i=1}^{[s/(g(h)h)]} ||\mathbf{A}_i^h|| + c_2 \sup_j ||\mathbf{A}_j^h||||\mathbf{A}_i^h|| > c_1] + \delta$$

for $h \le h_0$. Therefore, using (58), we find that $\exists\ c_1 > 0$ such that

$$\lim_{h\to 0} \mathbb{P}[\int_0^s ||\mathcal{A}^h(v)||dv > c_1] = 0. \tag{60}$$

Note also that for some $c_3 > 0$

$$\int_0^s ||\mathcal{A}(v,h)||dv < c_3 \tag{61}$$

since the coefficients a are bounded. In view of (55), (56) and (61) we find that $\exists\ c_4 > 0$ such that

$$\max\{||\mathbf{X}^{-1}||, ||\mathbf{X}||\} < c_4 \tag{62}$$

and from (60) that $\exists\ c_5 > 0$ so that

$$\lim_{h\to 0} \mathbb{P}[\sup_{0\le s\le t} ||\mathbf{X}^h(s)|| > c_5] = 0. \tag{63}$$

We find using (58) that $\exists\ c_6 > 0$ such that $\forall\ \delta > 0\ \ \exists\ h_2 > 0$ so that

$$\begin{aligned}
&\mathbb{P}[\sup_{0\le s\le L} ||\int_0^s \mathcal{A}^h(v) - \mathcal{A}(v,h)dv|| > \epsilon] \\
&\le \mathbb{P}[\sup_{0\le s\le L} ||\sum_{i=1}^{[s/(g(h)h)]} \mathbf{A}_i^h + \mathbf{B} \sup_{1\le i\le [L/(g(h)h)]} ||\mathbf{A}_i^h|| - \int_0^s \mathcal{A}(v,h)dv|| > \epsilon] + \delta,
\end{aligned}$$

for $h \le h_2$ with $||\mathbf{B}|| < c_6$. The bound in (27) then gives

$$\lim_{h\to 0} \mathbb{P}[\sup_{0\le s\le L} ||\int_0^s \mathcal{A}^h(v) - \mathcal{A}(v,h)dv|| > \epsilon] = 0. \tag{64}$$

From (57) and the above it then follows that

$$\lim_{h\to 0} \mathbb{P}[\sup_{0\le s\le L} ||\tilde{\mathbf{X}}^h(s)|| > \epsilon] = 0$$

and we have shown (54). Recall that

$$d_k^{N_s+k} = D_k^{N_s+k}\ \Pi_s^h$$

with $N_s = [s/(g(h)h)]$ and

$$\Pi_s^h = \prod_{m=1}^{[s/(g(h)h)]} \tau_m^h.$$

Finally, by using Lemma E.1 that gives the magnitude of Π_s^h and the result of Section D that bounds the relative magnitude of the reflected mode, we obtain Theorem 5.1.

Appendix D. The reflected mode.

In (5) we decompose the wavefield in terms of up- and a down-propagating wave components. Note that if the wave enters a homogeneous section with $\zeta(x) = \bar{\zeta}$ for $x > L$, then trivially the reflected wave component U vanishes for $x > L$ and the wave field is given in terms of the down-propagating wave component only. As we now show the reflected wave component will be small in general.

Note first that from (21) it follows

$$U_{2j}^{i+1} = \sum_{n=0}^{j} r_{i+1-2(j-n)}^h \prod_{k=1}^{n} \tau_{i-1-2(j-k)}^h\ D_{2(j-n)}^{i-n}, \tag{65}$$

where

$$\prod_{k=1}^{0} := 1.$$

We parameterize the vector of wave components at the front by

$$\tilde{\mathbf{D}}_j^i = [D_0^{i-j}, D_2^{i-j+1}, \cdots, D_{2j}^i]'.$$

Observe that

$$\prod_{k=1}^{n} \tau_{i-1-2(j-k)}^h \le 1.$$

Let $i \in \{0, \cdots, [L/(g(h)h)]\}$, then we find

$$U_{2j}^{i+1} \le \{\sup_{i+1-2j\le k\le i+1} |r_k^h|\}\ ||\tilde{\mathbf{D}}_j^i||.$$

From (19) and (21) we get the uniform bound:

$$|D_j^i| \le 1. \tag{66}$$

Thus, in view of (31) we find that for all $\epsilon > 0$ and $j \in \{0, \cdots, K\}$

$$\lim_{h\to 0} \mathbb{P}[\sup_{1\le i\le [L/(g(h)h)]} |U_{2j}^i| > \epsilon] = 0,$$

and that (29) is satisfied.

Appendix E. A bound on transmission.

We show how the magnitude of the solution of (23) can be bounded. Recall that

$$d_k^{N_s+k} = D_k^{N_s+k}\ \Pi_s^h$$

with $N_s = [s/(g(h)h)]$. Thus, in view of (66), we need to characterize the magnitude of Π_s^h.

LEMMA E.1. *The condition (27) implies that for all* $\epsilon > 0$

$$\lim_{h\to 0} \mathbb{P}[\sup_{0<s<L} |\ln(\Pi_s^h) + \int_0^s a(0, v/g(h), h)\ dv/2| > \epsilon] = 0, \tag{67}$$

with

$$\Pi_s^h = \prod_{m=1}^{[s/(g(h)h)]} \tau_m^h = \prod_{m=1}^{[s/(g(h)h)]} \sqrt{1-|r_m^h|^2}. \tag{68}$$

Proof. Note first that we can write

$$\ln\sqrt{1-|r_m^h|^2} = -\frac{|r_m^h|^2(1+v_m^h)}{2},$$

with

$$|v_m^h| \le |r_m^h|^2 \tag{69}$$

if $r_m^h < 1/2$. Observe next

$$\begin{aligned}
&\mathbb{P}[\sup_{0<s<L} |\ln(\Pi_s^h) + \int_0^s a(0, v/g(h), h)\ dv/2| > \epsilon] \\
&\le \mathbb{P}[\sup_{0<s<L} \frac{1}{2}|\sum_{m=1}^{[s/(g(h)h)]} |r_m^h|^2 - \int_0^s a(0, v/g(h), h)\ dv| + \frac{1}{2}\sup_m |v_m^h| \sum_{m=1}^{[s/(g(h)h)]} |r_m^h|^2 > \epsilon].
\end{aligned}$$

Let $\delta > 0$ be given, then from (27), (31) and (69) it follows that we can choose $h_0 > 0$ such that for $h \le h_0$

$$\mathbb{P}[\sup_{0<s<L} \frac{1}{2}\{\sup_m |v_m^h| \sum_{m=1}^{[s/(g(h)h)]} |r_m^h|^2\} > \epsilon/2] < \delta/2.$$

Therfore, for $h \le h_0$

$$\begin{aligned}
&\mathbb{P}[\sup_{0<s<L} |\ln(\Pi_s^h) + \int_0^s a(0, v/g(h), h)\ dv/2| > \epsilon] \\
&\le \delta/2 + \mathbb{P}[\sup_{0<s<L} \frac{1}{2}|\sum_{m=1}^{[s/(g(h)h)]} |r_m^h|^2 - \int_0^s a(0, v/g(h), h)\ dv| > \epsilon/2].
\end{aligned}$$

The result (67) then follows from (27). □

Appendix F. Limiting pulse shape and the Central Limit Theorem.

Recall that in the small h limit the impulse response of the random medium is characterized by the solution of (25). The matrix $\bar{\mathbf{A}}$ in (25) is lower triangular and Toeplitz and we find

$$\begin{aligned}\mathcal{D}(T,h) &= \exp(-\int_0^T \bar{\mathbf{A}}(s,h)\ ds)\ \mathbf{e}_1 \\ &= \exp(-\lambda(T,h))\exp(\lambda(T,h)\mathcal{Q}(T,h))\ \mathbf{e}_1\end{aligned}$$

using a parameterization analogous to the one in Section 5.3. Note that $\mathcal{Q}$ is a strictly lower triangular Toeplitz matrix and $\lambda(T,h) = \int_0^T \bar{\mathbf{A}}(s,h)_{(1,1)}\ ds$, where $\bar{\mathbf{A}}(s,h)_{(1,1)}$ is the main diagonal entry of the matrix $\bar{\mathbf{A}}(s,h)$. For some important random media models the first column of the matrix $\mathcal{Q}$, denote it $\mathbf{q}$, has non-negative entries and defines a discrete density supported on the non-negative integers. This is the case if for instance the random medium is Markovian. We want to characterize $\mathcal{D}$:

$$\mathcal{D} = \mathcal{D}(\lambda) \ = \ \exp(-\lambda)\exp(\lambda\mathcal{Q}(\lambda))\ \mathbf{e}_1 \ = \ \sum_{k=0}^{\infty}\exp(-\lambda)\ \frac{\lambda^k}{k!}\ \mathbf{q}_\lambda^{k*} \tag{70}$$

in the limit of large $\lambda = \lambda(T,h) = \int_0^T \mathcal{A}(s,h)_{(1,1)}\ ds$, corresponding to large travel time depths. Note that in (70) we made use of the fact that multiplication with $\mathcal{Q}$ corresponds to a discrete convolution. This formulation shows that if indeed $\mathbf{q}_\lambda$ defines a discrete distribution, then we can regard $\mathcal{D}$ as the distribution of a random sum supported on the non-negative integers. It follows that the pulse has constant area as it travels. By the formulas for the moments of a random sum we find that then the mean of $\mathcal{D}$ is $\lambda m(\lambda)$ and the variance $\lambda(v(\lambda)+m(\lambda)^2)$ when $m(\lambda)$ and $v(\lambda)$ are respectively the mean and variance associated with $\mathbf{q}_\lambda$. The next theorem shows that the normalized random sum converges in distribution to the standard Normal, hence, the wave pulse attains the Gaussian shape as it penetrates deep into the medium.

LEMMA F.1. *Let $\mathbf{q}_\lambda$ define a discrete distribution with mean $m(\lambda) \le \overline{m}$ and variance $0 < \underline{v} \le v(\lambda) \le \overline{v}$ and S_λ be distributed as a random sum according to*

$$\sum_{k=0}^{\infty} p_k^\lambda \mathbf{q}_\lambda^{k*}$$

with $p_k^\lambda = \exp(-\lambda)\lambda^k/k!$. Then, in the large λ limit

$$X_\lambda = \frac{S_\lambda - \lambda m(\lambda)}{\sqrt{\lambda(v(\lambda)+m(\lambda)^2)}} \tag{71}$$

converges in distribution to a standardized zero mean normal random variable.

Proof. Let

$$\exp(im(\lambda)t)\phi_\lambda(t)$$

be the characteristic function of $\mathbf{q}_\lambda$. The characteristic function of $S_\lambda/\sqrt{\lambda}$ is then

$$\begin{aligned}&\exp\{-\lambda + \lambda[\exp(im(\lambda)t/\sqrt{\lambda})\ \phi_\lambda(t/\sqrt{\lambda})]\} \\ &= \exp\{-\lambda + \lambda[1 + i\frac{m(\lambda)t}{\sqrt{\lambda}} - \frac{v(\lambda)t^2}{2\lambda} - \frac{m(\lambda)^2t^2}{2\lambda}] + o(1)\}\end{aligned}$$

for λ large. Thus, the characteristic function associated with X_λ defined in (71) is

$$\exp(-t^2/2 + o(1)),$$

in the λ large limit. Hence, Lemma F.1 follows in view of Theorem 26.3 in [2]. □

Note also that the distribution of $S_\lambda/\sqrt{\lambda}$ can be approximated by the distribution of a random sum of Gaussian random variables. The following lemma gives this characterization of S_λ.

LEMMA F.2. *Let p_k^λ, $\mathbf{q}_\lambda$ and S_λ be defined as in Lemma F.1. Let E_X denote expectation with respect to the distribution of $X_\lambda = S_\lambda/\sqrt{\lambda}$ and E_g denote expectation with respect to the distribution defined by:*

$$g_\lambda(x) = \sum_{k=0}^{\infty} p_k^\lambda \frac{\eta((x-\mu_k)/\sigma_k)}{\sigma_k} \tag{72}$$

where $\eta(\cdot)$ is the standard normal distribution, $\mu_k = km(\lambda)/\sqrt{\lambda}$, $\sigma_k^2 = kv(\lambda)/\lambda$ and $m(\lambda)$ and $v(\lambda)$ are defined as in Theorem F.1. Then

$$lim_{\lambda\to\infty}(E_g[u] - E_X[u]) = 0 \tag{73}$$

for every bounded continuous function u.